Lithos 160–161 (2013) 55–67

Contents lists available at SciVerse ScienceDirect

Lithos

journal homepage: www.elsevier.com/locate/lithos

Elemental responses to subduction-zone metamorphism: Constraints from the North Qilian Mountain, NW China

Yuanyuan Xiao [a,*], Yaoling Niu [a,b,**], Shuguang Song [c], Jon Davidson [a], Xiaoming Liu [d]

[a] Department of Earth Sciences, Durham University, Durham, DH1 3LE, UK
[b] School of Earth Sciences, Lanzhou University, Lanzhou 730000, China
[c] MOE Key Laboratory of Orogenic Belts and Crustal Evolution, School of Earth and Space Sciences, Peking University, Beijing 100871, China
[d] State Key Laboratory of Continental Dynamics, Department of Geology, Northwest University, Xi'an 710069, China

ARTICLE INFO

Article history:
Received 5 April 2012
Accepted 2 November 2012
Available online 6 December 2012

Keywords:
Subduction-zone metamorphism
North Qilian Mountain
Elemental behaviors
Arc magmatism

ABSTRACT

Subduction zone metamorphism (SZM) and behaviors of chemical elements in response to this process are important for both arc magmatism and mantle compositional heterogeneity. In this paper, we report the results of our petrographic and geochemical studies on blueschist and eclogite facies rocks of sedimentary and basaltic protoliths from two metamorphic sub-belts with different metamorphic histories in the North Qilian Mountain, Northwest China. The protolith of low-grade blueschists is basaltic in composition and is most likely produced in a back-arc setting, while the protoliths of high-grade blueschists/eclogites geochemically resemble the present-day normal and enriched mid-oceanic ridge basalts plus some volcanic arc rocks. The meta-sedimentary rocks, including meta-graywacke, meta-pelite, meta-chert and marble, show geochemical similarity to global oceanic (subducted) sediments. Assuming that high field strength elements (HFSEs) are relatively immobile, the correlated variations of rare earth elements (REEs) and Th with HFSEs suggest that all these elements are probably also immobile, whereas Pb and Sr are mobile in rocks of both basaltic and sedimentary protoliths during SZM. Ba, Cs and Rb are immobile in rocks of sedimentary protoliths and mobile in rocks of basaltic protolith. The apparent mobility of U in rocks of basaltic protolith may be inherited from seafloor alterations rather than caused by SZM.

On the basis of *in situ* mineral compositional analysis (both major and trace elements), the most significant trace element storage minerals in these subduction-zone metamorphic rocks are: lawsonite, pumpellyite, apatite, garnet and epidote group minerals for REEs, white micas (both phengite and paragonite) for large ion lithophile elements, rutile and titanite for HFSEs. The presence and stability of these minerals exert the primary controls on the geochemical behaviors of most of these elements during SZM. The immobility of REEs, Th and U owing to their redistribution into newly formed minerals suggests that subduction-zone dehydration metamorphism will not contribute to the enrichment of these elements in arc magmatism. These observations require the formation and contribution of supercritical fluids or hydrous melts (these can effectively transport the aforementioned incompatible elements) from greater depths to arc magmatism. In addition, the overall sub-chondritic Nb/Ta ratio retained in rutile-bearing eclogites indicates that the subducting/subducted residual ocean crust passing through SZM cannot be responsible for the missing Nb (relative to Ta) in the bulk silicate earth.

1. Introduction

Subduction zone metamorphism (SZM) is important for both arc magmatism and mantle compositional heterogeneity. Experimental studies and studies on natural rocks have significantly improved our understanding of SZM processes over the past twenty years.

The recognition of hydrous minerals (e.g., lawsonite, zoisite, and phengite) stable under ultrahigh pressure (UHP) conditions indicates fluid preservation beyond the stability of amphibole during SZM (e.g., Pawley and Holloway, 1993; Poli and Schmidt, 2002), and has encouraged a new model combining both stepwise and continuous reactions occurring simultaneously in different parts of the subducting slab (Schmidt and Poli, 2003), instead of simple discontinuous dehydrations in previous models (e.g., Tatsumi, 1986; Tatsumi and Eggins, 1995; Tatsumi and Kogiso, 1997). Furthermore, UHP hydrous phases can largely conserve their preferential chemical elements until their breakdown (e.g., El Korh et al., 2009; Feineman et al., 2007; Hermann, 2002; Hermann and Rubatto, 2009), thus the mobility of these preferentially hosted elements is not simply controlled by major dehydration reactions (e.g., transition from blueschist to eclogites facies) during SZM (e.g., Hermann et al., 2006; Spandler et al., 2003). The mobility of elements is a function of many factors, including the stability of mineral

* Corresponding author. Tel.: +86 183 9210 3987.
** Correspondence to: Y. Niu, Department of Earth Sciences, Durham University, Durham, DH1 3LE, UK. Tel.: +44 19 1334 2311; fax: +44 19 1334 2301.
E-mail addresses: xiaoy806@gmail.com, yuanyuan.xiao@durham.ac.uk (Y. Xiao), yaoling.niu@durham.ac.uk (Y. Niu).

0024-4937/$ – see front matter © 2012 Elsevier B.V. All rights reserved.
http://dx.doi.org/10.1016/j.lithos.2012.11.012

phases at given conditions (Niu and Lesher, 1991), physical and chemical properties of fluids (e.g., compositional variations, supercritical fluids, and hydrous melts; Hermann et al., 2006; Manning, 2004; Rapp et al., 2010), and mechanisms of fluid flow as well as the fluid/rock ratios (John et al., 2008; Zack and John, 2007). Hence, a given element may show different behaviors during SZM. For example, by comparing eclogite and the gabbroic protolith, John et al. (2004) argues for light rare earth elements (LREEs) being mobile during subduction zone eclogitization, yet others found that they are immobile at the presence of epidote group minerals (e.g., El Korh et al., 2009; Spandler et al., 2003, 2004; Xiao et al., 2012). Furthermore, although experimental studies have demonstrated that high field strength elements (HFSEs) are immobile during SZM, which is consistent with inferences from arc magma geochemistry (Kogiso et al., 1997), John et al. (2008) argued that these elements are mobile during SZM. All these new views of possibly varying elemental behaviors during SZM clearly contrast with the globally consistent elemental characteristics of arc magmas (i.e., depletion of Nb–Ta–Ti and enrichment of Ba, Rb, Cs, U etc.), which has been widely accepted as resulting from subducting-slab dehydration (McCulloch and Gamble, 1991; Stolper and Newman, 1994). It follows that if HFSEs can indeed be mobilized during SZM, other processes must have been at work and responsible for the globally consistent geochemical characteristics of arc magmas. Therefore, further detailed and systematic studies of subduction zone metamorphic rocks are required to better understand how chemical elements respond to SZM.

We report here the results of this detailed petrographic and geochemical study on blueschist and eclogite facies rocks of seafloor protoliths from the North Qilian Mountain. Specifically, using both bulk-rock and mineral compositional data, we attempted to understand elemental behaviors in response to the specific metamorphic history of the North Qilian subduction-zone complex, and to evaluate the most likely geochemical consequences of SZM and their potential contributions to arc magmatism (Xiao et al., 2012).

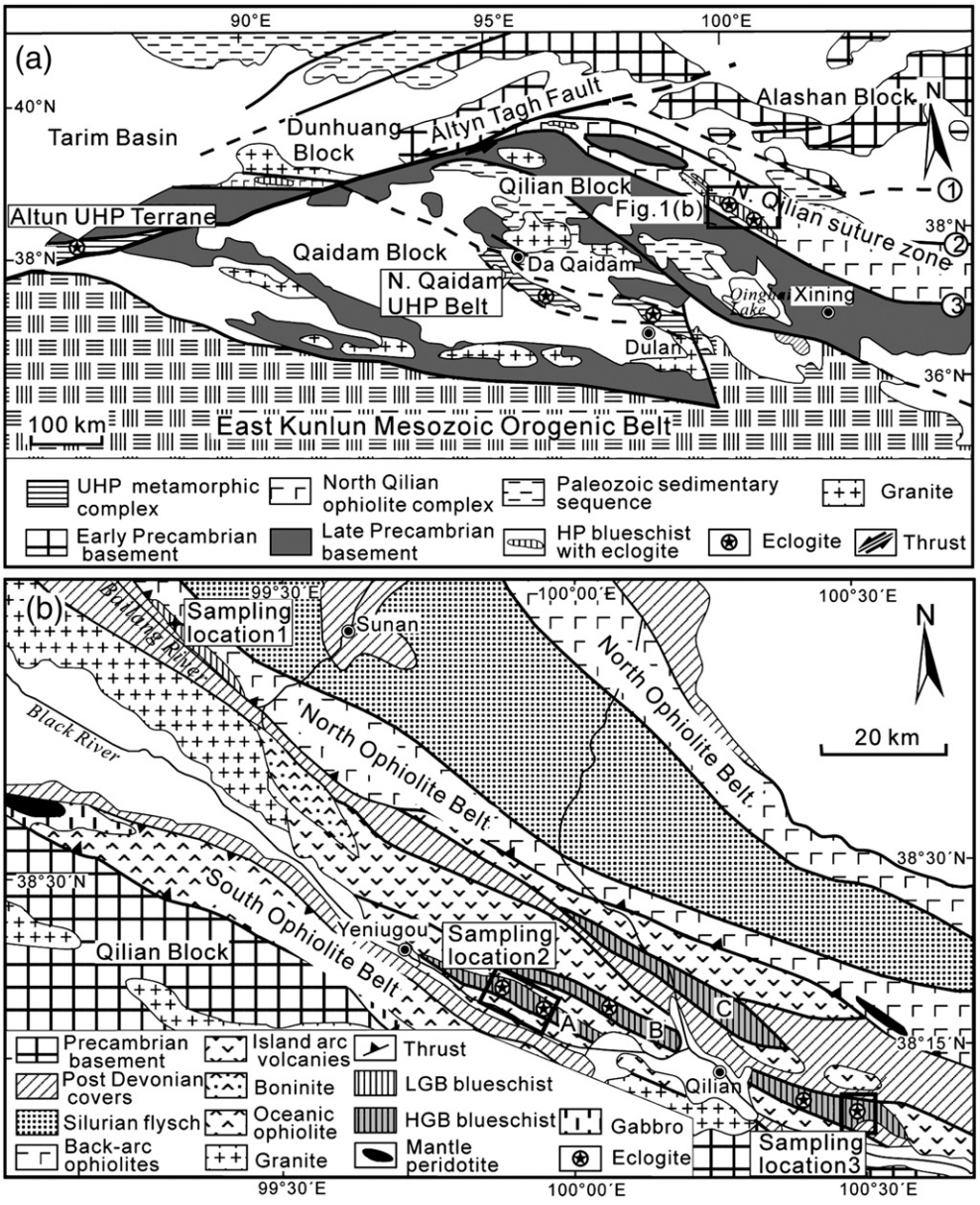

Fig. 1. (a) Simplified geological map of Qilian–Qaidam Mountain region in NW China. ①-Longshoushan Fault; ②, ③-northern and southern boundary faults of North Qilian Suture Zone. (b) Outcrop of North Qilian Suture Zone including sampling locations (after Song et al., 2007, 2009; Xia and Song, 2010; Wu et al., 1993). Sampling location 1 in Sunan is along the low grade blueschist belt (LGB), while sampling location 2 and sampling location 3 near Qilian County are within slices (slice A and slice B) of high grade blueschist/eclogite belt (HGB).

2. Geological background of North Qilian Mountain and samples

2.1. Geological setting of North Qilian Mountain

We choose to carry out this study on subduction-zone metamorphic rocks from the Palaeozoic North Qilian oceanic-type Suture Zone (ONQ, or North Qilian Mountain; Fig. 1) in northwest China. The ONQ, about 80–100 km wide, extends NW-SE for over 800 km along the northern margin of the Tibetan Plateau (Fig. 1a; Song et al., 2006, 2009, in press) and offset to the west by the Altyn Tagh Fault. The ONQ comprises an ophiolite complex (e.g., Xia et al., 2012), island-arc volcanic rocks, high-pressure (HP) blueschists and eclogites, Silurian flysch formation, Devonian molasse, and Carboniferous to Triassic sedimentary cover sequences (e.g., Feng and He, 1995; Song et al., 2006, 2012; Wu et al., 1993; Xia et al., 2003; Fig. 1b).

The ONQ comprises two sub-parallel metamorphic sub-belts (Fig. 1b), one is a high grade blueschist/eclogite metamorphic belt (HGB) with higher metamorphic temperature and pressure of up to 460–510 °C at 2.2–2.6 GPa (Song et al., 2007), the other is a low-grade blueschist metamorphic belt (LGB) with only 320–375 °C and 0.75–0.95 GPa (Lin et al., 2010; Zhang et al., 2009) or 250–350 °C at 0.6–1.1 GPa (Song et al., 2009). The protoliths of blueschist and eclogite facies rocks from HGB include graywacke, marble, chert and basaltic rocks (Song et al., 2007, 2009; Wu et al., 1993), while basaltic rocks are the dominant protolith rock type for those from LGB (Song et al., 2009; see further comparison of their mineral assemblages in Table DR1). Based on the previous studies (e.g., Song, 1997; Song et al., 2009; Wu et al., 1993; Zhang et al., 2009), the HGB is considered to be produced by the subduction of mature ocean seafloor, while the formation of the LGB may be attributed to the subduction of back-arc basin seafloor.

The existing studies, including the recognition of lawsonite-bearing eclogite/blueschist (e.g., Song et al., 2007; Wu et al., 1993; Zhang and Meng, 2006; Zhang et al., 2007) and Mg-carpholite-bearing metamorphic rocks of pelitic protolith (Song et al., 2007), indicate that the ONQ is one of the oldest (~560–440 Ma) orogenic belts preserving rock assemblages of a cold intra-oceanic subduction zone (see Song et al., 2007, 2009; Zhang et al., 2007). The ONQ ophiolite complex is of Early Palaeozoic age (e.g., 568–495 Ma; Shi et al., 2004; Song et al., 2012; Tseng et al., 2007; Yang et al., 2002; Zhang et al., 2007), and the ancient Qilian Ocean already existed in the Early Cambrian and may have been opened in the Late Proterozoic (~710 Ma; Song et al., 2009, 2012). The timing of subsequent eclogitization (~490–460 Ma, e.g., Song et al., 2009; Zhang et al., 2007) is consistent with the age of island-arc volcanic rocks (~486–445 Ma; Liu et al., 2006; Wang et al., 2005; Wu et al., 1993; Xia et al., 2003) and the spreading history of the back-arc basin (Song et al., 2012; Xia and Song, 2010; Xia et al., 2012). The back-arc basin spreading and eclogitization have been interpreted as resulting from northward subduction of Qilian Ocean seafloor, the dehydration of which further led to the formation of arc volcanic rocks in the Ordovician time (e.g., Song et al., 2006; Xia et al., 2003). The Ar–Ar dating of glaucophane and phengite from retrograde blueschist (~462–440 Ma, cooling ages; Liou et al., 1989; Song et al., 2007, 2009; Wu et al., 1993; Zhang et al., 1997) and meta-pelite (454–442 Ma, Liu et al., 2006) in HGB, together with the occurrence of Silurian flysch formation and Devonian molasse, mark the end of oceanic seafloor subduction at ~440 Ma (e.g., Song et al., 2006, 2012). Together with the inferred progressive P-T path (Fig. 2), the thermal gradient during the subduction is estimated to be 6–7 °C/km (Song et al., 2009).

2.2. Samples and petrography

Sample locations are shown in Fig. 1b, and GPS position for each sample is given in Table DR2. Rocks of basaltic protoliths are sampled from both LGB and HGB, while rocks of sedimentary protoliths are only sampled from HGB. The representative mineral assemblages in distinctive types of metamorphic rocks from LGB and HGB are summarized in Table DR1 and shown in Fig. 3 with a detailed petrographic description.

3. Analytical methods and data

Sample powders for the whole rock analysis were prepared in the Langfang Laboratory of the Chinese Geological Survey. Saw marks and the weathered surfaces were thoroughly removed from hand specimens before ultrasonically cleaned in an ultrasonic bath in distilled water. A corundum jaw was used to crush cleaned samples into chips. The fresh rock chips were then selected and finally pulverized using agate ball mills.

Bulk-rock compositional analysis was done at Northwest University, China. Bulk-rock major elements were analyzed using X-ray fluorescence (Rigaku RIX 2100 XRF) on fused glass disks. Analytical precision for major elements is better than 5% as determined from duplicate analyses.

Bulk-rock trace elements were analyzed using inductively coupled plasma mass spectrometry (Agilent 7500a ICPMS). To ensure complete digestion, an $HF + HNO_3$ mix was used to dissolve sample powders in high-pressure Teflon bombs at 190 °C for 48 h. Rh was added to the sample solutions as an internal standard to monitor signal drift during analysis (see procedures in Rudnick et al., 2004). The United States Geological Survey (USGS) reference materials (AGV-2, BHVO-2, BCR-2 and GSP-1) were used to ensure both analytical precision and accuracy (Table DR3). Analytical accuracies (relative error, RE) in terms of AGV-2 for all the trace elements are within ±10%, although the RE of several elements in terms of other reference materials is large, i.e., 52.7% Be, −17.2% Cr and −13.2% Ni for BCR-2, −26.2% Sc and −20.1% Pb for BHVO-2 (Table DR3), even more elements in terms of GSP-1, as a result of the much lower contents of these elements in GSP-1 (Liu et al., 2007). The precisions (relative standard deviation, RSD) for almost all the trace elements are better than 5% as determined from duplicate analyses (Table DR3). The analytical bulk-rock compositional data are given in Table DR4 and Table DR5.

Mineral major elements were analyzed using a JXA-8100 electron probe micro-analyzer (EPMA) at Chang'an University, China. The analyses were done using accelerating voltage of 15 kV and 10 nA probe current with 1 micron beam diameter. Standards used for

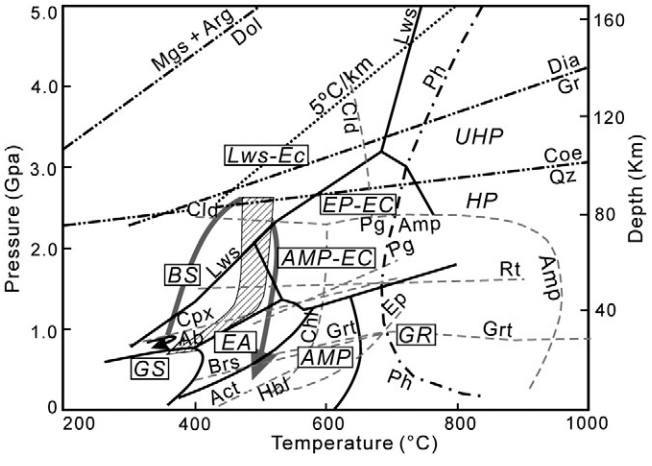

Fig. 2. Estimated P-T paths for rocks of basaltic protoliths from HGB and LGB of North Qilian Mountain. Metamorphic facies boundaries are from Liou et al. (2004). The wide hatched arrow for HGB is from Song et al. (2007), while the thin black arrow for LGB is from to Zhang et al. (2009). The gray curve is the schematic P-T path for rocks of basaltic protoliths from UHP metamorphic belt of Western Tianshan in NW China (see Xiao et al., 2012). The mineral abbreviations used in this paper are referred to Whitney and Evans (2010), except Ca — carbonate; Czs — (clino)zoisite; Mica — white micas; and Opa — Opaque minerals.

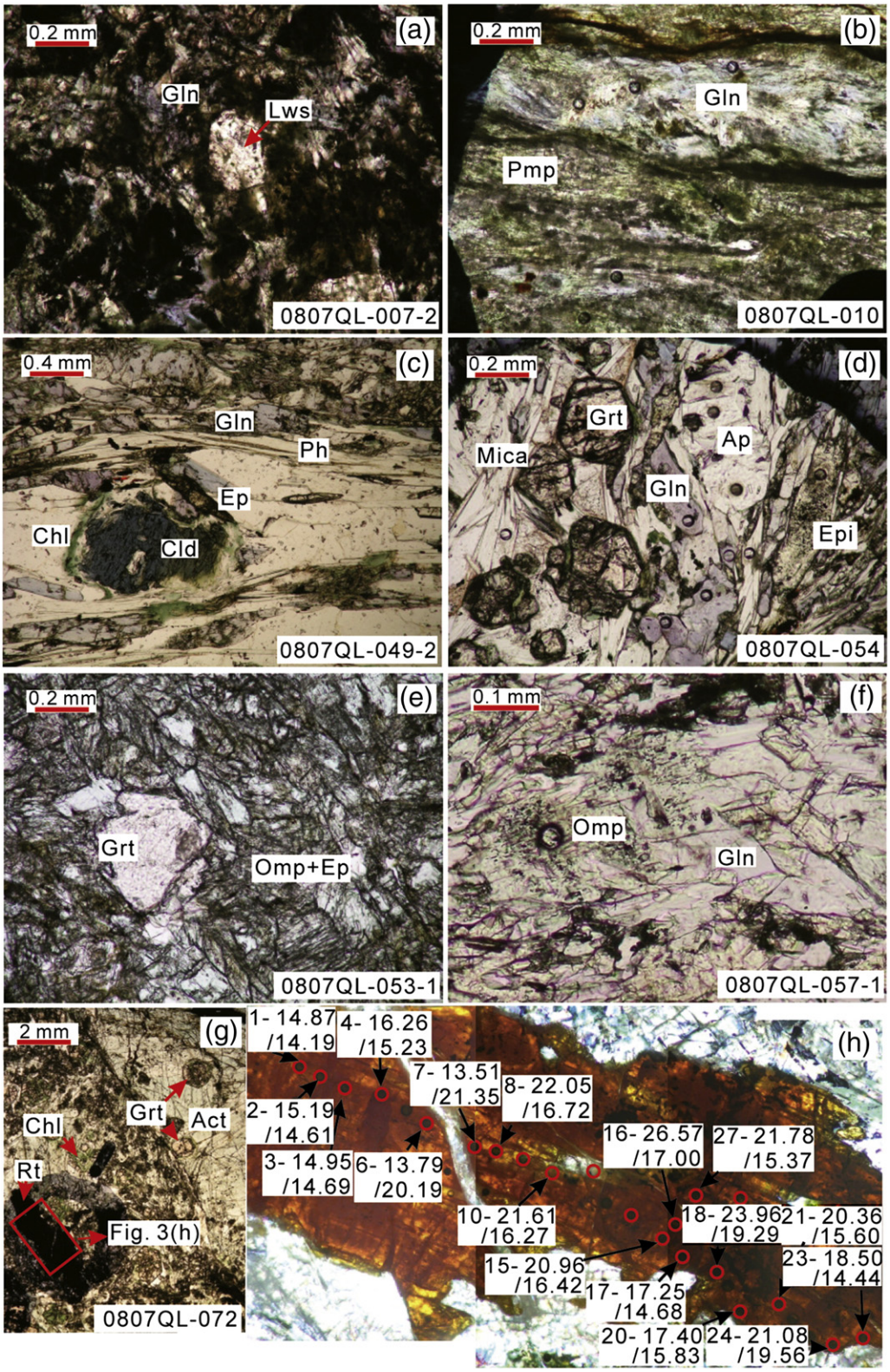

Fig. 3. Photomicrographs of representative samples from both LGB (a–b) and HGB (c–h). All the photos are taken under PPL. (a). Lawsonite glaucophanite. Lawsonite, characteristically box-shaped, exists as porphyroblasts in fine grained matrix. (b). Glaucophane pumpellyite schist. Interbedded glaucophane and pumpellyite define the clear schistosity. (c). Grt–Cld–Gln–Ph schist, the representative of meta-pelite, characterized by the common occurrence of chloritoid porphyroblasts. (d). Blueschist–facies meta-sedimentary rock. The high proportions of quartz and white micas in mineral assemblages are distinctive features of meta-sedimentary rocks. (e–f). Eclogitic blueschist, composed of garnet porphyroblast and the matrix made up of omphacite, glaucophane and epidote. 0807QL-057-1 is also used for bulk-rock composition reconstruction in Fig. 7a. (g). Amphibolite. One large rutile is found up to 2 mm length. (h) is the close up of the rutile shown in (g). Nb/Ta and Zr/Hf ratios using LA-ICPMS are labeled next to analyzed point (x — y/z; x = the number of the analyzed point; y = the Nb/Ta ratio; z = the Zr/Hf ratio).

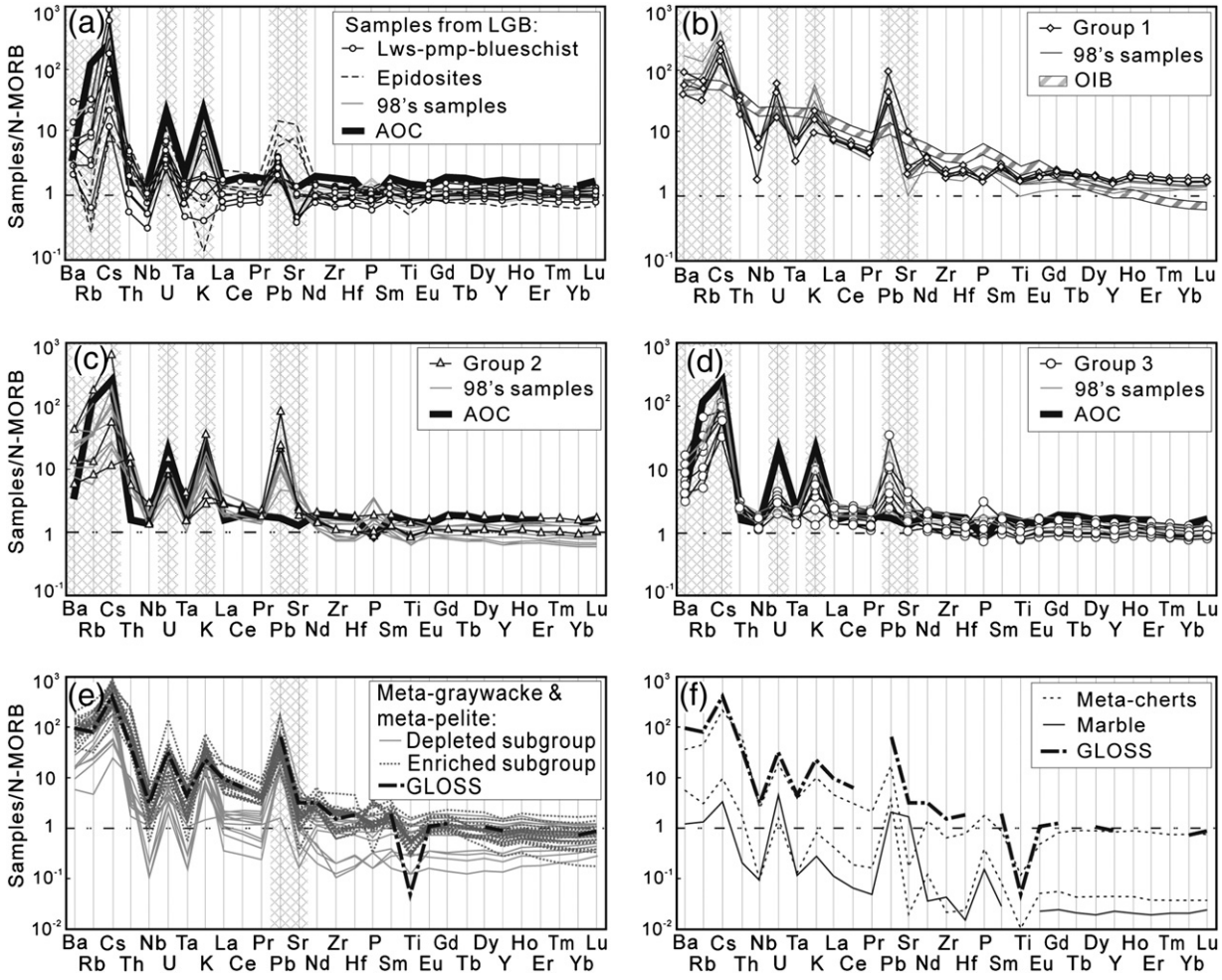

Fig. 4. N-MORB normalized multi-element distributed diagrams for bulk-rock compositions of metamorphic rocks from LGB (a) and HGB (b–f) of ONQ. Mobile elements discussed in the relevant text of Section 6.2 are indicated with hatches in (a–e). The gray curves in (a–d) represent 1998's samples from Song et al. (2009) and Lavis (2005). Group classification for mafic blueschist and eclogites from HGB (b–d) is discussed in the Section 5.2.1. Oceanic island basalts (OIB; after Sun and McDonough, 1989) and the altered oceanic crust (AOC; after Kelley et al., 2003) are plotted in (b) and (a, c–d) respectively for comparison with meta-basaltic rocks. Global oceanic subducted sediment (GLOSS; Plank and Langmuir, 1998) is plotted in (e–f) for comparison with meta-sedimentary rocks.

calibration are: albite for Na, quartz for Si, orthoclase for K, apatite for P and Ca, magnetite for Fe, pyrophanite for Mn and Ti, chromite for Cr and Fe, forsterite for Mg, and jadeite for Al (Minwu Liu, 2009, personal communication). Mineral major element compositional data using EPMA are given in Table DR6.

LA-ICPMS is used for *in situ* analyses of both major and trace elements in anhydrous minerals (garnet, omphacite, rutile, titanite, and feldspar), using the innovative method without adding internal standards developed by Liu et al. (2008) at both Northwest University and China University of Geosciences in Wuhan. Instead of calibrating

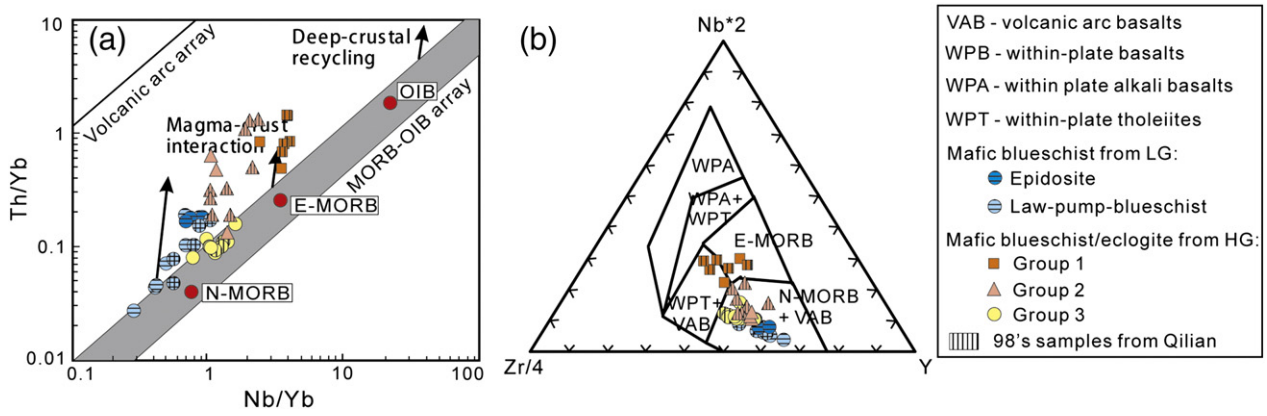

Fig. 5. Discrimination diagrams for blueschists and eclogites of basaltic proliths from both LGB and HGB. (a) Th/Yb vs. Nb/Yb (after Pearce, 2008). OIB, E-MORB and N-MORB (Sun and McDonough, 1989) are plotted for comparison. (b) Nb*2-Zr/4-Y (after Meschede, 1986).

against one element of known concentration (e.g., analyzed by EPMA) as the internal standard, the innovative method uses the actual analyses of all the unknown elements normalized to 100% in each spot/run and an ablation yield correction factor (AYCF) obtained based on multiple reference materials. The advantage of this method lies in its avoiding uncertainties associated with mineral compositional heterogeneity. The plots in Fig.DR1 reveal that major element contents of anhydrous minerals using LA-ICPMS and calibrated by the method reported in Liu et al. (2008) are within 10% relative deviation from the data by EPMA, except for elements with very low contents (e.g., TiO_2 in garnet), which is excellent. For hydrous minerals (muscovite, paragonite, lawsonite, epidote group minerals, pumpellyite, apatite, amphiboles, chloritoid, and chlorite), a major element by EPMA (Si was chosen) was used as the internal standard for *in situ* LA-ICPMS trace elements. In terms of a synthetic reference glass GSE-1G (which contains high trace element concentrations ranging from several ppm to primarily 100 s ppm; Guillong et al., 2005; Jochum et al., 2005), the accuracy is evaluated to be within ±5% (except P), and the precision is better than 10% for almost all the analyzed major and trace elements. Mineral trace element compositional data obtained using LA-ICP-MS are given in Table DR7 and Table DR8 for anhydrous and hydrous minerals respectively. The major element compositional data by LA-ICPMS for anhydrous minerals have also been reported in Table DR7.

4. Bulk-rock geochemistry and tectonic discrimination

In the following, we discuss our samples and data, together with the data on bulk-rock composition in the literature on ONQ samples from the same sampling location (Lavis, 2005; Song et al., 2009).

4.1. Geochemistry of metamorphic rocks from LGB

The LGB samples are mainly epidosite, lawsonite glaucophanite and glaucophane pumpellyite schist, and are basaltic in composition with 45.91 to 53.67 wt.% SiO_2 (Table DR4). Different hydrous minerals, especially high H_2O-bearing minerals (e.g., pumpellyite, lawsonite, chlorite, containing up to 12.5 wt.% H_2O), are widespread in mineral assemblages of rocks from LGB, and thus resulted in commonly high bulk loss on ignition (LOI) (>2.33 wt.%; see Table DR4), which is even higher in rocks with carbonate, e.g., 0807QL-015-2 (25 vol.% carbonate and 7.01 wt.% LOI). Epidosite is dominated by epidote (>40 vol.%, see Table DR2) with varying amount of carbonate, and thus contains higher CaO (15.15–16.66 wt.%) than the other two lithologies in LGB (i.e., 5.10–8.74 wt.%), but lower MgO (2.03–3.83 wt.% vs. 6.75–8.80 wt.%). Consistent with the higher contents of Sr and Pb in epidote than in pumpellyite and glaucophane, epidosite also shows higher Sr and Pb contents.

In the N-type MORB-normalized multi-element diagram (Fig. 4a), except for Ba, Rb, Cs, U, K, Pb and Sr, which are assumed to be mobile

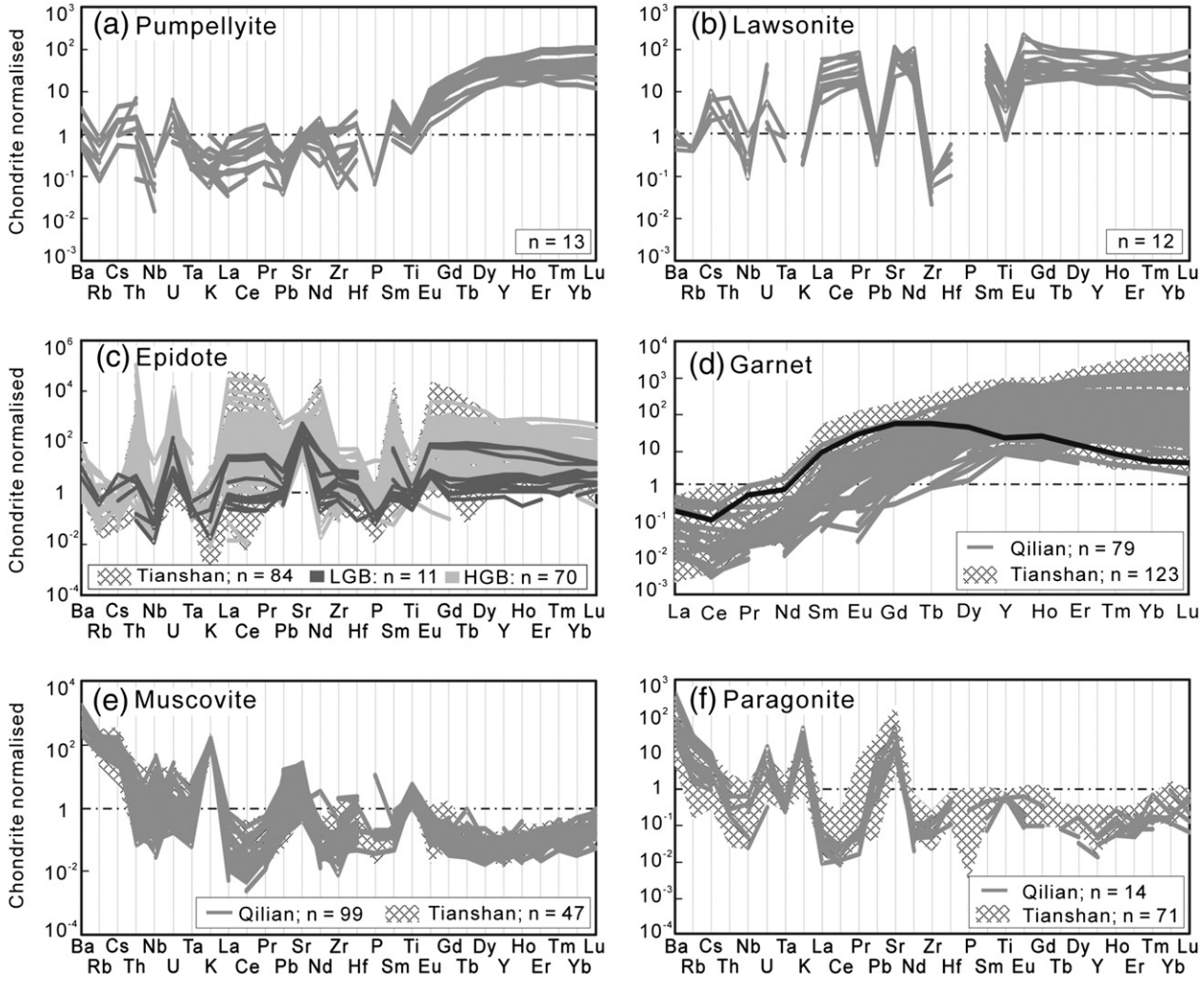

Fig. 6. Chondrite-normalized multi-element distributed diagrams for minerals in blueschist and eclogite facies rocks from LGB and HGB. The values of chondrite are referred to Sun and McDonough (1989). The analytical results of relevant minerals in blueschist/eclogite facies rocks from Western Tianshan, NW China, are also plotted for comparison, which are represented by the hatched areas in (c–f, h, j–k). The highlighted curve in (d) is used for discussion in Section 5.2.

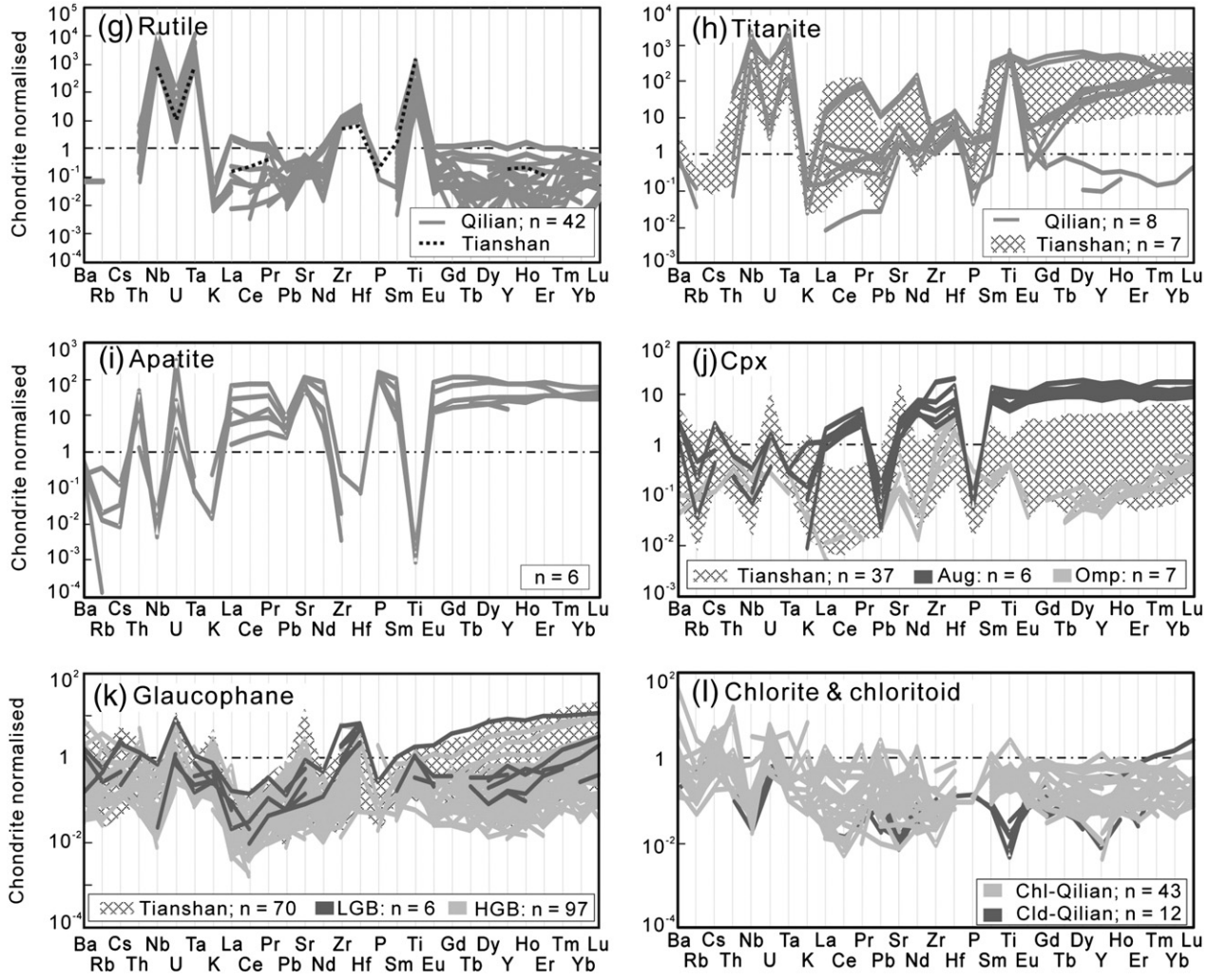

Fig. 6 (*continued*).

during subduction zone metamorphism (or prior seafloor weathering effects, e.g., Kelley et al., 2003; Staudigel et al., 1995), the generally flat elemental patterns of LGB metamorphic rocks reflect their geochemical affinity to N-type MORB. However, assuming high field strength elements (HFSEs) and HREEs are immobile during SZM, the plots in Fig. 5a define a trend slightly deviated from MORB – oceanic island basalts (OIB) array. As Pearce (2008) suggested, this deviation indicates that these samples also possess arc-related geochemical signatures. Therefore, the protoliths of LGB metamorphic rocks are probably originated from a back-arc basin (vs. an oceanic ridge setting) as previously suggested (Song et al., 2009), which is also consistent with the presence of wehrlite intrusions (vs. troctolite; the indicator of the high fluid content during crystallization; Niu, 2005) and high volume of volcanic breccias and terrigenous-sedimentary rocks in the field (Jiugequan) (e.g., Song et al., 2009).

4.2. Geochemistry of metamorphic rocks from HGB

4.2.1. Blueschists/eclogites

The SiO_2 content of blueschists and eclogites from HGB varies from 45.14 to 50.06 wt.% (Table DR5). Despite the presence of hydrous phases like epidote group minerals, glaucophane (which contain ~2.0–2.2 wt.% H_2O, Poli and Schmidt, 1995) and white micas (~4.3–4.6 wt.% H_2O, Poli and Schmidt, 1995), the absence of H_2O-rich phases (e.g., lawsonite, and pumpellyite) and abundant anhydrous minerals (e.g., garnet and omphacite) explain the overall lower LOI in HGB meta-basaltic rocks than those in LGB rocks. However, the presence of carbonate in several meta-basaltic samples has led to the high LOI (e.g., up to 3.90 wt.% in 0807QL-053-2, Table DR5). All the HGB rocks of basaltic protolith may be readily divided into three groups in terms of their geochemistry (Table DR5 and Figs. 4,5): samples from Group 1 have high TiO_2 and K_2O, and low MgO; samples from Group 2 have high MgO and Al_2O_3; samples from Group 3 show high CaO and low total Fe_2O_3. Consistently, all the phengite-rich eclogites reported by Song et al. (2009) belong to Group 1, while epidote-rich eclogites in their study have been included in Group 2 and Group 3.

Samples from Group 1 show higher large ion lithophile elements (LILEs), Th, and overall REEs ($\sum$REEs), and higher LREE/HREE ratios (Fig. 4b). Group 1 and Group 2 samples plot in the E-MORB and N-MORB fields in Fig. 5b, respectively. However, they deviate from the MORB-OIB array in Fig. 5a, and show pronounced depletions in Nb and Ta (Fig. 4b). Thus, these rocks reflect an arc signature and may have been assimilated with continental material. As for Group 3, all samples show a flat pattern of REEs and HFSEs with variably enriched Ba, Rb, Cs, U, K, Pb and Sr (Fig. 4d), and plot in the MORB-OIB array (Fig. 5a), suggesting an N-MORB-like protolith. All of these indicate that protoliths of HGB meta-basaltic rocks possess geochemical features

of N- to E-MORB from ridges or near-ridge seamounts (Song et al., 2009), influenced by arc-related material (Group 1 and Group 2).

4.2.2. Meta-sedimentary rocks

Meta-sedimentary rocks, relative to meta-basaltic rocks from HGB, show large major element compositional variations. They have generally higher SiO_2 and LOI, but lower MgO and TiO_2 (Table DR5). The large amount of phengite accounts for the high K_2O in theses rocks (e.g., up to 5.61 wt.% K_2O in 0807QL-067 for 45 vol.% phengite). The multi-element patterns of meta-sedimentary rocks (Fig. 4e,f), including meta-graywacke, meta-pelite, meta-chert and marble, are generally similar to that of global oceanic subducted sediments (GLOSS; Plank and Langmuir, 1998). Meta-graywackes and meta-pelites show two subgroups in terms of Th and U contents and ratios of REEs (Fig. 4e); the subgroup with higher Th and U possesses higher LREE/HREE ratios. The great variability of these elements reflects the complex provenance for the protoliths of meta-sedimentary rocks.

5. Mineral geochemistry

5.1. Mineral major elements

We analyzed garnet, white micas (both muscovite and paragonite), lawsonite, epidote group minerals, rutile, titanite, amphiboles, clinopyroxene, chlorite, chloritoid, and pumpellyite using EPMA (Table DR6).

Garnet crystals are dominantly almandine and generally show normal zoning of pyrope (increasing rimward), reflecting prograde growth (e.g., Lü et al., 2009). The tiny garnet crystals (~40 μm) in samples from Baishiya contain very high spessartine (e.g., garnet from 0807QL-043 as shown in Table DR6). The clinopyroxene in meta-basaltic rocks from LGB is inherited magmatic augite, while the clinopyroxene in meta-basaltic rocks from HGB are omphacitic. Most analyzed amphibole crystals are glaucophane, but some calcic amphiboles (e.g., actinolite, and tremolite) and sodic calcic amphiboles (e.g., barroisite), commonly as retrograde product, have also been analyzed in some samples (nomenclature from Leake et al., 1997). The composition of epidote group minerals is highly variable. FeOt and Al_2O_3 are negatively correlated as the result of $Al–Fe^{3+}$ substitution. White micas are predominantly phengite with minor paragonite, which is distinguished in terms of Na/K ratios.

5.2. Mineral trace elements

We found that the most important trace element hosts are pumpellyite (Fig. 6a), lawsonite (Fig. 6b), epidote (Fig. 6c), garnet (Fig. 6d), phengite (Fig. 6e), paragonite (Fig. 6f), rutile (Fig. 6g), titanite (Fig. 6h), and apatite (Fig. 6i). Albite can also contain high Sr (Table DR7). Omphacite (Fig. 6j), glaucophane (Fig. 6k), chloritoid (Fig. 6l) and chlorite (Fig. 6l) have low contents of almost all the analyzed trace elements. Representative analytical data are given in Table DR7 for anhydrous minerals and Table DR8 for hydrous minerals.

Pumpellyite is an important index mineral in low-grade metamorphic rocks, but has rarely been analyzed for trace elements (only Spandler, 2003 reported some). It has high elevated abundances of heavy REEs (HREEs; Fig. 6a), similar to those in garnet (Fig. 6d). Sr and Ba are present at ppm levels, along with detectable Th, U, Cs, Rb and Pb. Lawsonite is characterized by consistently high REEs and Sr (Fig. 6b). REE fractionation is minimal ($[LREEs/HREEs]_{chondrite} \leq 1$). Epidote group minerals show variable REEs, Th and U (Fig. 6c), and consistently high Sr and Pb. Garnet is characterized by variably high HREEs (Fig. 6d). Some garnet grains show high middle-REEs (MREEs; $[MREEs > HREEs]_{chondrite}$, e.g., the highlighted curve in Fig. 6d), which is likely inherited from the precursor phases (e.g., MREE-rich amphiboles, titanite) during high pressure prograde metamorphism (Spandler et al., 2003). Alternatively, presence of other potential mineral phases, like zircons locally can strongly draw HREEs, resulting in HREE depletion of the nearby garnet because zircons have higher Kd (HREEs) than garnet (e.g., Rubatto and Hermann, 2007). Apatite shares similar trace element patterns to lawsonite, except for its characteristic high P as major element and slightly higher Pb, Th and U but lower Ti and Cs (Fig. 6i vs. 6b).

Both phengite and paragonite commonly contain high Ba, Cs, Rb, Pb, Sr, Li (10 s of ppm) and Be (several ppm). In addition, phengite contains one order of magnitude higher Ba, Cs, Rb than paragonite, whereas paragonite has higher Pb and Sr (Fig. 6e vs. 6f; also see Table DR8). Phengite from meta-sedimentary rocks has obviously higher Pb and Sr than those from meta-basaltic rocks, and also relatively more scattered Ba, Cs and Rb, which are especially variable among white micas from different rocks.

Rutile and titanite contain high amounts of Nb and Ta (Fig. 6g & h). Titanite can also have variably high REEs with varying REE fractionation patterns ($[MREEs > HREEs]_{chondrite}$ or $[MREEs < HREEs]_{chondrite}$ in Fig. 6h). Albite is depleted in all the trace elements but Sr, and to a less extent, Ba (Table DR7). Although omphacite in eclogitic rocks from HGB contains low contents of almost all the analyzed trace elements, several analyzed magmatic clinopyroxene relicts (i.e., augite) in metamorphic rocks from LGB show a HREE-enriched pattern (more than 10 × chondrite; Fig. 6j).

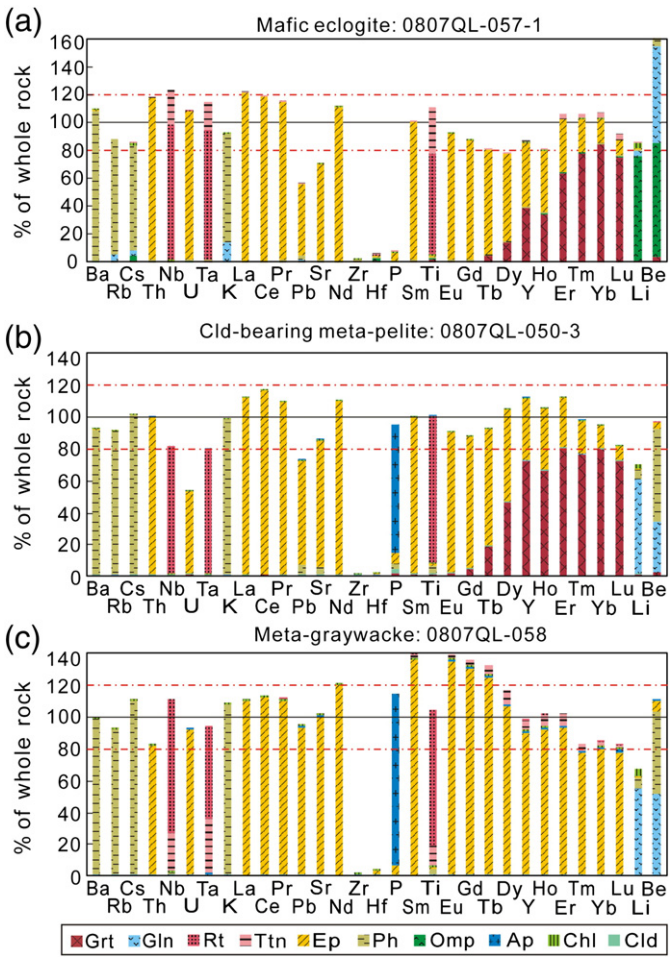

Fig. 7. Reconstructed trace element budgets compared with analyzed bulk-rock compositions for three representative rocks from HGB of ONQ, with different protolith lithologies, i.e., eclogite, meta-pelite and meta-graywacke. The black horizontal line represents the analyzed bulk-rock composition, and two dotted-dashed lines in each panel represent ±20% deviation respectively. Bars with different patterns represent different mineral hosts. Most trace element budgets are comparable with the analyzed bulk-rock trace element contents. However, because it is hard to find zircon for analysis, there are big gaps for Zr and Hf in reconstructions. The big gap for P in (a) is also attributed to the tiny crystal size or the highly heterogeneous distribution of apatite.

6. Discussion

6.1. Trace element budgets

We used estimated mineral modes (Table DR2) and analyzed mineral trace element contents (e.g., Table DR7 and Table DR8) to reconstruct trace element budgets for three distinctive protolith lithologies from HGB (Fig. 7). The consistency of reconstructed compositions with analyzed bulk-rock compositions for most trace elements illustrates the reliability of our reconstruction, although uncertainties exist due to the highly variable mineral compositions, the heterogeneous mineral distributions and the presence of non-analyzed accessory minerals (e.g., zircon). Although different rock types have different bulk-rock compositions and different mineral assemblages, the same mineral in different rock types still shows generally the similar capability to host elements (Fig. 7).

Since paragonite is rare in metamorphic rocks from the ONQ (especially compared with the studies on those from Western Tianshan) and as it contains lower LILEs than phengite (Table DR8), we conclude that phengite accommodates almost all the K, Ba, Rb and Cs in the bulk rock. A significant fraction of the Pb and Sr budgets could also reside in phengite (Fig. 7b). All Ti, Nb and Ta are hosted in rutile, and to a lesser extent in titanite. Apatite, commonly in meta-sedimentary rocks (Fig. 7b,c), contains more than 90% P, but because of its low modal abundances, the contribution of apatite to the budgets of Th, U, Pb, Sr and REEs in the bulk-rock composition is insignificant although apatite can contain moderate abundance of these elements (Fig. 6i). Almost all the M-HREEs are dominated by garnet and epidote group minerals. When garnet is absent (e.g., blueschist-facies meta-graywacke in Fig. 7c), epidote group minerals become more significant for M-HREEs. All the Th, U and LREEs, plus some Pb and Sr, are hosted in epidote group minerals. Chlorite, glaucophane and omphacite contribute little to bulk-rock trace element budgets (except for Li and Be), although they are volumetrically the major phases in these rocks.

For metamorphic rocks from LGB, because of the inherited magmatic texture and the fine grain size, the reconstruction is not possible. However, considering the mineral trace element contents (Fig. 6) and the relative mineral abundances, the most important hosts for REEs, Th, U, Pb and Sr are lawsonite and epidote, apatite to a lesser extent. Pumpellyite is especially important for HREEs, and probably titanite can also host some REEs. LILEs are hosted in white micas. Albite and carbonate may also host some Sr and Pb (also see van der Straaten et al., 2008).

6.2. Element mobility and their controls

Assuming HFSEs are immobile, their correlation coefficients with elements having similar incompatibility in basaltic protoliths would reflect the mobility or immobility of these elements (see Niu, 2004; Xiao et al., 2012; Fig. 8). If their correlations are insignificant, it means that this element must have been mobilized during later metamorphism. Otherwise, it indicates that the element is similarly immobile to the reference HFSE. Fig. 8 shows the correlation coefficients of the immobile incompatible elements Nb and Zr with other trace elements. The elements along the x-axis are sorted in terms of decreasing incompatibility from left to right following the order reported by Niu and Batiza (1997). Therefore, Fig. 8a and b suggest that for rocks of basaltic protoliths from both LGB and Group 3 of HGB, Li, Ba, Rb, Cs, Pb and Sr are mobile, while Be, REEs and HFSEs are immobile. This is broadly similar to our observations on metamorphic rocks from Western Tianshan (Xiao et al., 2012). As for Th, the clearly positive trends between Nb and Th for Group 3 of HGB, especially for rocks of basaltic protoliths from LGB (Fig. 9a), suggest the immobility of Th. U is moderately mobile, especially in Group 3 of HGB (Fig. 8a,b), in contrast to our previous study on Tianshan samples where U shows considerable immobility (Xiao et al., 2012).

For meta-sedimentary rocks (Fig. 8c), Th, U, REEs and HFSEs are clearly immobile, while Pb, Sr and Li are mobile. Although the correlations of Ba, Rb, Cs and K with HFSEs are not so high, they still define a broad positive trend for LILEs vs. HFSEs (e.g., Nb vs. Rb in Fig. 9b)

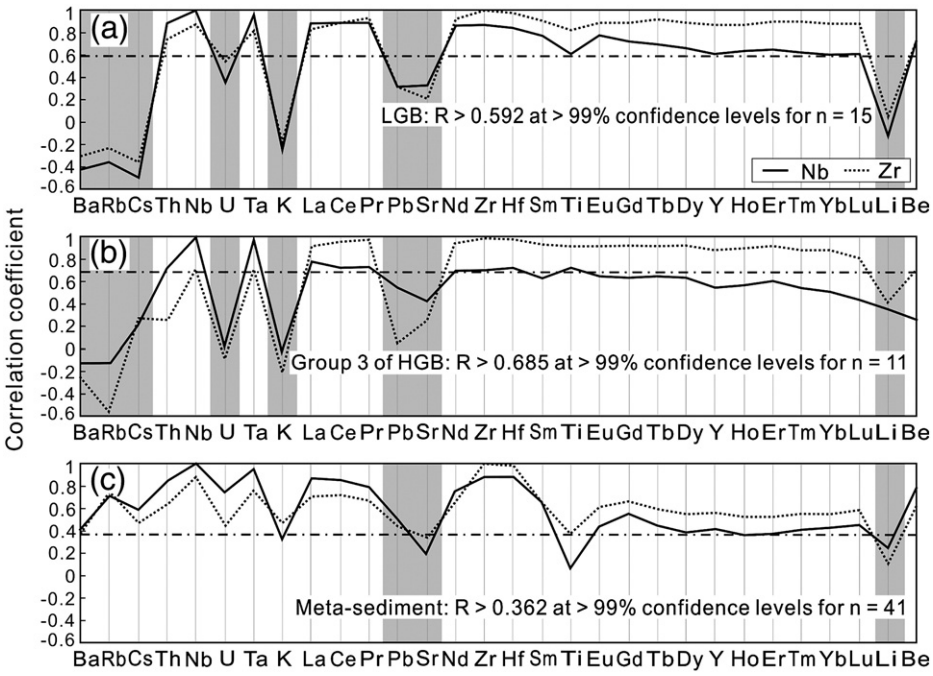

Fig. 8. Correlation coefficient diagrams of Nb and Zr with other trace elements for (a) rocks from LGB, (b) rocks from HGB (Group 3 is chosen as its clear origin), and (c) meta-sedimentary rocks from North Qilian Mountain (the methodology is referred to Niu, 2004 and Xiao et al., 2012). Elements along the X-axis are ordered in terms of decreasing incompatibility from left to right. Two immobile elements (Nb and Zr) are chosen considering their different incompatibilities during magmatic processes. The dotted-dashed lines represent the minimum significant correlation coefficients for a certain sample size above 99% confidence levels (referred to critical values of Pearson's correlation coefficient using one-tail test). Therefore, generally, elements with correlation coefficients plotted below the dotted-dashed lines are considered mobile, which has been constrained by the gray areas, whereas those plotted above are considered immobile.

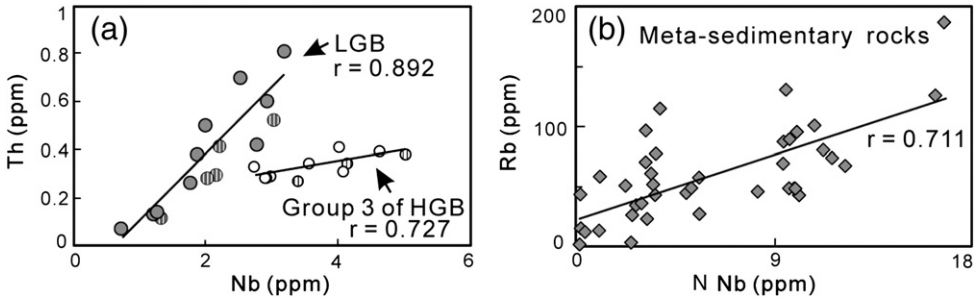

Fig. 9. Elemental co-variation diagrams. (a) Nb vs. Th for rocks from LGB and Group 3 of HGB. The hatched circles represent 1998's samples from Song et al. (2009) and Lavis (2005). (b) Nb vs. Rb for rocks of sedimentary protoliths from HGB. The clear trend for the correlation between Nb and Rb in meta-sedimentary rocks indicates the moderate immobility (vs. mobility) of Rb, Ba and Cs in meta-sedimentary rocks (similar trends could also be obtained for Cs and Ba with Nb, although the trend with Ba is not so obvious).

showing moderate immobility, in contrast with their behavior in the meta-basaltic rocks.

The unclear correlations of U with those assumed immobile elements for rocks of basaltic protoliths (Fig. 8a,b) indicate that U may have been mobilized since the last magmatic process, which involved both seafloor alteration and subsequent subduction-zone metamorphism. Our study on Western Tianshan samples shows that U is immobile as are Th and HFSEs (Xiao et al., 2012), which experienced similar cold subduction zone metamorphism to HGB metamorphic rocks from the ONQ (Fig. 2). Therefore, it is less likely that U is mobilized during SZM.

One of the most significant geochemical features caused by hydrothermal alteration is the general enrichment of U in altered/weathered seafloor basalts (e.g., Kelley et al., 2003; Staudigel et al., 1995). Although the immobility of U in blueschists/eclogites from Western Tianshan may reflect the absence of U enrichment during seafloor alteration (the heterogeneity of hydrothermal alteration) and/or the possibility of erosion the altered seafloor materials during subduction (which may result in the input of only unaltered seafloor materials into subduction zones), the mobility of U in this study may reflect enrichment caused by this seafloor modification. Some Ba, Rb, Cs and K may have also been enriched by seafloor hydrothermal alteration before their further modifications during SZM (e.g., Kelley et al., 2003; Staudigel et al., 1995).

During prograde SZM, with the transition from pumpellyite-prehnite facies to epidote eclogite facies, HREEs are mainly transferred from pumpellyite (Fig. 6a) and augite (Fig. 6j) to garnet (Fig. 6d). Meanwhile, as more epidote is produced at the expense of lawsonite, LREEs are redistributed between them conservatively. HFSEs are completely transferred from titanite to rutile. For Pb and Sr, although they could be hosted and redistributed among albite, apatite, white micas, carbonate, and epidote to different extents, a portion of them may be released with fluids due to the breakdown of epidote during the main reaction of the blueschist-to-eclogite transition: 13 Gln + 6 Czs = 9 Prp + 26 Jd + 12 Di + 19 Qz + 16 H_2O, as evidenced by experimental work (Feineman et al., 2007). Ba, Cs and Rb, dominantly hosted in phengite, are mobile in rocks of basaltic protoliths from both LGB and HGB, and may have been released partly before the formation of phengite. In rocks of sedimentary protoliths, however, because white micas are already present in sedimentary protoliths, these elements could be conserved.

6.3. The preservation of Nb/Ta ratio during SZM

We have analyzed some well-crystallized and preserved rutile grains (Fig. 3g,h). As rutile and titanite host almost all the Nb and Ta in the bulk rock (Fig. 7), the composition of these two minerals

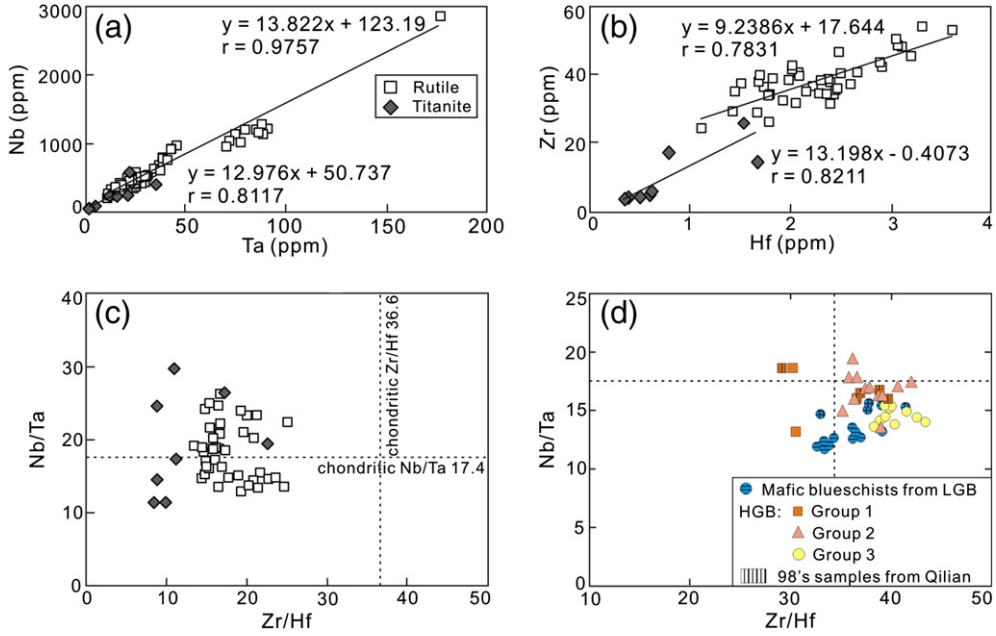

Fig. 10. (a–b) The co-variation diagrams of Nb vs. Ta and Zr vs. Hf for both rutile and titanite. Slops of the linear correlation represent the geometrical mean of Nb/Ta and Zr/Hf ratios for rutile and titanite respectively. (c) Plots of Nb/Ta vs. Zr/Hf ratios for rutile and titanite. The Nb/Ta ratios in rutile and titanite are both superchondritic and subchondritic. All the Zr/Hf ratios in rutile and titanite are subchondritic. (d) Bulk-rock Nb/Ta vs. Zr/Hf ratios. The hatched symbols represent those 1998's samples (see Lavis, 2005; Song et al., 2009). The dashed lines in (c–d) denote the chondritic values of Nb/Ta (= 17.4; Jochum et al., 2000) and Zr/Hf (= 36.6; Sun and McDonough, 1989) respectively.

can help to understand possible Nb–Ta fractionation in rutile-bearing eclogites.

The arithmetic mean Nb/Ta ratio in rutile and titanite are similar; 18.50 ± 3.78 (1σ; n = 42) in rutile vs. 19.50 ± 6.95 (1σ; n = 8) in titanite. However, the geometrical mean of Nb/Ta ratio in rutile is higher than that in titanite (i.e., the slope in Nb–Ta space; 13.822 vs. 12.976, Fig. 10a). Zr and Hf contents of rutile and titanite are also plotted in Fig. 10b. The Nb/Ta ratio is highly variable, and shows both superchondritic and subchondritic values in both rutile and titanite, while the Zr/Hf ratio in both Ti-bearing minerals is only subchondritic (Fig. 10c). The variability of Nb/Ta and Zr/Hf ratios can be found even within a single crystal (Fig. 3h), and this may be closely associated with the HFSE contents of minerals nearby (most likely titanite), at the expense of which rutile is formed.

Bulk-rock Nb/Ta and Zr/Hf ratios plotted in Fig. 10d display no obvious superchondritic Nb/Ta ratio. Therefore, subducted rutile-bearing oceanic crust cannot be the missing Nb (relative to Ta) reservoir responsible for the subchondritic Nb/Ta in bulk silicate Earth (Niu, 2012; Rudnick et al., 2000).

7. Implications for subduction zone magmatism

The arc basalts differ from MORB in their enrichment in LILEs and depletion in HFSEs, or the characteristic "arc signature" (McCulloch and Gamble, 1991; Stolper and Newman, 1994). This arc signature, plus the high water contents, has been the primary evidence for slab-dehydration induced mantle wedge melting for arc magmatism (e.g., McCulloch and Gamble, 1991). If this interpretation is correct, we can assume that without subduction zone dehydration metamorphism, there would be no arc magmatism.

Our studies on samples both from North Qilian Mountain (this study) and Western Tianshan, NW China (Xiao et al., 2012) revealed the mobility of Ba, Rb, Cs, Pb and Sr in rocks of basaltic protolith and the immobility of REEs, Th, U and HFSEs in rocks of both sedimentary and basaltic protoliths in response to the subduction-zone metamorphism, which is broadly consistent with the estimated mobility/immobility inferred for the petrogenesis of arc lavas (e.g., Tamura et al., 2007). The observed enrichments of LILEs in arc lavas (Fig. 11) are thus most likely attributed to their mobility in released fluids from subducting/subducted oceanic crust with or without terrestrial sediments. The strongly depleted Nb and Ta in arc magmas may result from their retention in rutile in subducted slab rocks (Kogiso et al., 1997; McCulloch and Gamble, 1991).

Owing to the redistribution into newly formed minerals, REEs, Th and U are immobile in both meta-basaltic and meta-sedimentary rocks during SZM (although U shows its mobility during seafloor alteration in this study), which is well demonstrated by those rocks from Western Tianshan (Xiao et al., 2012). Thus, these elements are not expected to be carried into the mantle wedge by fluids. Although the geochemical behavior of LILEs in SZM and their enrichments in arc lavas seem to be consistent with the model of slab-dehydration induced mantle wedge melting, the relative enrichments in LREEs, Th and U commonly observed in IAB (Fig. 11), yet their immobility revealed from SZM rocks suggests that some additional or other medium are at work (vs. simple effects of slab fluid transport).

We suggest that the transport of the apparently fluid-immobile Th and U, and to a lesser extent, LREEs, to mantle wedges may have accomplished through supercritical fluids or hydrous melts from greater depths for arc magmatism, rather than simple subduction zone slab dehydration metamorphism. Supercritical fluids or hydrous melts, generated at depths beyond those represented by our samples (no less than 75 km deep for metamorphic rocks from Western Tianshan, Xiao et al., 2012) is necessarily required for arc magmatism (e.g., Hermann and Rubatto, 2009; Kessel et al., 2005).

8. Conclusions

(1) Consistent with the observations on HP and UHP metamorphic rocks from Western Tianshan, the North Qilian Mountain samples also show that Ba, Rb and Cs are mobile in meta-basaltic rocks and immobile in meta-sedimentary rocks, whereas REEs and HFSEs are immobile and Pb and Sr are mobile in both lithologies. Thus, Ba, Rb, Cs, Pb and Sr could contribute to the mantle wedge source regions of arc lavas through subducting slab derived aqueous fluids, while enrichments of Th and U and LREEs in arc lavas require transport through supercritical fluids or hydrous melts generated deeper than 75 km.

(2) Metamorphic mineral controls on element behavior are important during SZM. Phengite (and, to a lesser extent, paragonite) accommodates essentially all the Ba, Rb and Cs; titanite and rutile accommodate all the Nb and Ta, with titanite also hosting REEs, Th, U, Sr, and Pb; epidote and garnet are responsible for all the M-HREEs transferred from pumpellyite and augite that are stable in low grade metamorphic rocks; almost all the Th, U and LREEs, and a large proportion of the Sr and Pb are also hosted in epidote. Apatite, like lawsonite, can contain high concentrations of Th, U, Pb, Sr and REEs during SZM, but because of the low modal abundance of apatite (probably also lawsonite), epidote is still the dominant host for these elements.

(3) The Nb/Ta ratio in rutile varies significantly, probably as a result of competing effects of spatially coexisting phases on petrographic scales. The subchondritic Nb/Ta ratio in eclogites of the residual ocean crust protoliths indicates that the ocean crust, if subducted to the deep mantle, cannot be the Nb-rich reservoir needed to balance the missing Nb (i.e., the subchondritic Nb/Ta ratio) in the bulk silicate Earth.

Acknowledgments

This study was supported by the National Natural Science Foundation of China (grant numbers: 9101400, 41130314 to Yaoling Niu and

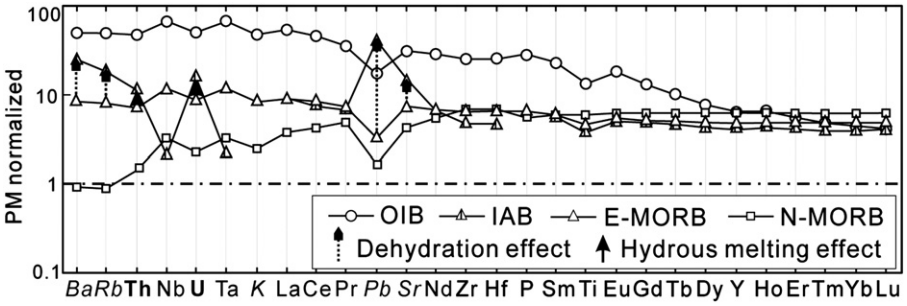

Fig. 11. Primitive mantle (PM) normalized multi-element distributed patterns for OIB and N-/E-MORB (after Sun and McDonough, 1989) and IAB (from Elliott, 2003). The elemental symbols in italic are those elements most likely controlled by dehydration process, while those in bold are elements that require supercritical fluids or hydrous melts for their enrichments in arc lavas.

40825007, 40821002 to Shuguang Song). The analyses were funded by the School of Earth Sciences, Lanzhou University, China. We thank Jianqi Wang, Ye Liu, professor Honglin Yuan, Kaiyun Chen, and Mengning Dai at the State Key Laboratory of Continental Dynamics of Northwest University in Xi'an, China for the help with bulk-rock compositional and LA-ICPMS analysis. We also thank professor Yongsheng Liu for supplying *ICPMSDATACAL* software. The discussion with professor Yongfei Zheng is also thanked. Comments from the editor in chief (Andrew Kerr) and two anonymous reviewers are gratefully appreciated and have helped to improve this paper.

Appendix A. Supplementary data

Supplementary data to this article can be found online at http://dx.doi.org/10.1016/j.lithos.2012.11.012.

References

El Korh, A., Schmidt, S.T., Ulianov, A., Potel, S., 2009. Trace element partitioning in HP-LT metamorphic assemblages during subduction-related metamorphism, Ile de Groix, France: a detailed LA-ICPMS Study. Journal of Petrology 50, 1107–1148.
Elliott, T., 2003. Tracers of the slab. Geophysical Monograph 138, 23–45.
Feineman, M.D., Ryerson, F.J., DePaolo, D.J., Plank, T., 2007. Zoisite-aqueous fluid trace element partitioning with implications for subduction zone fluid composition. Chemical Geology 239, 250–265.
Feng, Y., He, S., 1995. Research for geology and geochemistry of several ophiolites in the North Qilian Mountains, China. Acta Petrologica Sinica (in Chinese) 11, 125–146.
Guillong, M., Hametner, K., Reusser, E., Wilson, S.A., Gunther, D., 2005. Preliminary characterisation of new glass reference materials (GSA-1G, GSC-1G, GSD-1G and GSE-1G) by laser ablation-inductively coupled plasma-mass spectrometry using 193 nm, 213 nm and 266 nm wavelengths. Geostandards Geoanalytical Research 29, 315–331.
Hermann, J., 2002. Allanite: thorium and light rare earth element carrier in subducted crust. Chemical Geology 192, 289–306.
Hermann, J., Rubatto, D., 2009. Accessory phase control on the trace element signature of sediment melts in subduction zones. Chemical Geology 265, 512–526.
Hermann, J., Spandler, C., Hack, A., Korsakov, A.V., 2006. Aqueous fluids and hydrous melts in high-pressure and ultra-high pressure rocks: implications for element transfer in subduction zones. Lithos 92, 399–417.
Jochum, K.P., Stolz, A.J., McOrist, G., 2000. Niobium and tantalum in carbonaceous chondrites: constraints on the solar system and primitive mantle niobium/tantalum, zirconium/niobium, and niobium/uranium ratios. Meteorittics & Planet Science 35, 229–235.
Jochum, K.P., Willbold, M., Raczek, I., Stoll, B., Herwig, K., 2005. Chemical characterisation of the USGS reference glasses GSA-1G, GSC-1G, GSD-1G, GSE-1G, BCR-2G, BHVO-2G and BIR-1G using EPMA, ID-TIMS, ID-ICP-MS and LA-ICP-MS. Geostandards Geoanalytical Research 29, 285–302.
John, T., Scherer, E.E., Haase, K., Schenk, V., 2004. Trace element fractionation during fluid-induced eclogitization in a subducting slab: trace element and Lu–Hf–Sm–Nd isotope systematics. Earth and Planetary Science Letters 227, 441–456.
John, T., Klemd, R., Gao, J., Garbe-Schonberg, C.D., 2008. Trace-element mobilization in slabs due to non steady-state fluid–rock interaction: constraints from an eclogite–facies transport vein in blueschist (Tianshan, China). Lithos 103, 1–24.
Kelley, K.A., Plank, T., Ludden, J., Staudigel, H., 2003. Composition of altered oceanic crust at ODP Sites 801 and 1149. Geochemistry Geophysics Geosystem 4.
Kessel, R., Schmidt, M.W., Ulmer, P., Pettke, T., 2005. Trace element signature of subduction-zone fluids, melts and supercritical liquids at 120–180 km depth. Nature 437, 724–727.
Kogiso, T., Tatsumi, Y., Nakano, S., 1997. Trace element transport during dehydration processes in the subducted oceanic crust: 1. Experiments and implications for the origin of ocean island basalts. Earth and Planetary Science Letters 148, 193–205.
Lavis, S., 2005. Recycling in subduction zones: evidence from eclogites and blueschist of NW China. Cardiff University, pp. 1–245.
Leake, B.E., Woolley, A.R., Arps, C.E.S., Birch, W.D., Gilbert, M.C., Grice, J.D., Hawthorne, F.C., Kato, A., Kisch, H.J., Krivovichev, V.G., Linthout, K., Laird, J., Mandarino, J.A., Maresch, W.V., Nickel, E.H., Rock, N.M.S., Schumacher, J.C., Smith, D.C., Stephenson, N.C.N., Ungaretti, L., Whittaker, E.J.W., Youshi, G., 1997. Nomenclature of amphiboles: report of the subcommittee on amphiboles of the International Mineralogical Association, Commission on new minerals and mineral names. American Mineralogist 82, 1019–1037.
Lin, Y., Zhang, L., Ji, J., Wang, Q., Song, S., 2010. $^{40}Ar/^{39}Ar$ isochron ages of lawsonite blueschists from Jiuquan in the northern Qilian Mountain, NW China, and their tectonic implications. Chinese Science Bulletin 55, 2021–2027.
Liou, J.G., Wang, X., Coleman, R.G., Zhang, Z.M., Maruyama, S., 1989. Blueschists in major suture zones of China. Tectonics 8, 609–619.
Liou, J.G., Tsujimori, T., Zhang, R.Y., Katayama, I., Maruyama, S., 2004. Global UHP metamorphism and continental subduction/collision: the Himalayan model. International Geology Review 46, 1–27.
Liu, Y.-J., Neubauer, F., Genser, J., Takasu, A., Ge, X.-H., Handler, R., 2006. $^{40}Ar/^{39}Ar$ ages of blueschist facies pelitic schists from Qingshuigou in the Northern Qilian Mountains, western China. Island Arc 15, 187–198.
Liu, Y., Liu, X.M., Hu, Z.C., Diwu, C.R., Yuan, H.L., Gao, S., 2007. Evaluation of accuracy and long-term stability of determination of 37 trace elements in geological samples by ICP-MS. Acta Petrologica Sinica 23, 1203–1210.
Liu, Y.S., Hu, Z.C., Gao, S., Günther, D., Xu, J., Gao, C.G., Chen, H.H., 2008. In situ analysis of major and trace elements of anhydrous minerals by LA-ICP-MS without applying an internal standard. Chemical Geology 257, 34–43.
Lü, Z., Zhang, L.F., Du, J.X., Bucher, K., 2009. Petrology of coesite-bearing eclogite from Habutengsu Valley, western Tianshan, NW China and its tectonometamorphic implication. Journal of Metamorphic Geology 27, 773–787.
Manning, C.E., 2004. The chemistry of subduction-zone fluids. Earth and Planetary Science Letters 223, 1–16.
McCulloch, M.T., Gamble, J.A., 1991. Geochemical and geodynamicai constraints on subduction. Earth and Planetary Science Letters 102, 358–374.
Meschede, M., 1986. A method of discriminating between different types of mid-ocean ridge basalts and continental tholeiites with the Nb–Zr–Y diagram. Chemical Geology 56, 207–218.
Niu, Y.L., 2004. Bulk-rock major and trace element compositions of abyssal peridotites: implications for mantle melting, melt extraction and post-melting processes beneath mid-ocean ridges. Journal of Petrology 45, 2423–2458.
Niu, Y.L., 2005. Generation and evolution of basaltic magmas: some basic concepts and a new view on the origin of Mesozoic–Cenozoic basaltic volcanism in Eastern China. Geological Journal of China Universities 11, 9–46.
Niu, Y., 2012. Earth processes cause Zr–Hf and Nb–Ta fractionations, but why and how? RSC Advances.
Niu, Y.L., Batiza, R., 1997. Trace element evidence from seamounts for recycled oceanic crust in the Eastern Pacific mantle. Earth and Planetary Science Letters 148, 471–483.
Niu, Y.L., Lesher, C.M., 1991. Hydrothermal alteration of mafic metavolcanic rocks and genesis of Fe–Zn–Cu sulfide deposits, Stone Hill District, Alabama. Economic Geology and the Bulletin of the Society of Economic Geologists 86, 983–1001.
Pawley, A.R., Holloway, J.R., 1993. Water sources for subduction zone volcanism: new experimental constraints. Science 260, 664–667.
Pearce, J.A., 2008. Geochemical fingerprinting of oceanic basalts with applications to ophiolite classification and the search for Archean oceanic crust. Lithos 100, 14–48.
Plank, T., Langmuir, C.H., 1998. The chemical composition of subducting sediment and its consequences for the crust and mantle. Chemical Geology 145, 325–394.
Poli, S., Schmidt, M.W., 1995. H_2O transport and release in subduction zones: experimental constraints on basaltic and andesitic systems. Journal of Geophysical Research 100 (22,299-222,314).
Poli, S., Schmidt, M.W., 2002. Petrology of subducted slabs. Annual Review Earth Planet Science 30, 207–235.
Rapp, J.F., Klemme, S., Butler, I.B., Harley, S.L., 2010. Extremely high solubility of rutile in chloride and fluoride-bearing metamorphic fluids: an experimental investigation. Geology 38, 323–326.
Rubatto, D., Hermann, J., 2007. Experimental zircon/melt and zircon/garnet trace element partitioning and implications for the geochronology of crustal rocks. Chemical Geology 241, 38–61.
Rudnick, R.L., Barth, M., Horn, I., McDonough, W.F., 2000. Rutile-bearing refractory eclogites: missing link between continents and depleted mantle. Science 287, 278–281.
Rudnick, R.L., Gao, S., Ling, W.-l., Liu, Y.-s., McDonough, W.F., 2004. Petrology and geochemistry of spinel peridotite xenoliths from Hannuoba and Qixia, North China craton. Lithos 77, 609–637.
Schmidt, M.W., Poli, S., 2003. Generation of mobile components during subduction of oceanic crust. In: Rudnick, R.L. (Ed.), Treatise on Geochemistry. Elsevier, New York, pp. 567–591.
Shi, R., Yang, J., Wu, C., Wooden, J., 2004. First SHRIMP dating for the formation of the late Sinian Yushigou Ophiolite, North Qilian Mountains. Acta Geologica Sinica (in Chinese with English abstract) 78, 649–657.
Song, S., 1997. Tectonic evolution of subductive complex belts in the north Qilian mountains. Advance in Earth Sciences (in Chinese with English abstract) 12, 351–365.
Song, S.G., Zhang, L.F., Niu, Y.L., Su, L., Song, B., Liu, D.Y., 2006. Evolution from oceanic subduction to continental collision: a case study from the Northern Tibetan Plateau based on geochemical and geochronological data. Jounal of Petrology 47, 435–455.
Song, S.G., Zhang, L.F., Niu, Y., Wei, C.J., Liou, J.G., Shu, G.M., 2007. Eclogite and carpholite-bearing metasedimentary rocks in the North Qilian suture zone, NW China: implications for Early Palaeozoic cold oceanic subduction and water transport into mantle. Journal of Metamorphic Geology 25, 547–563.
Song, S., Niu, Y., Zhang, L., Wei, C., Liou, J.G., Su, L., 2009. Tectonic evolution of early Paleozoic HP metamorphic rocks in the North Qilian Mountains, NW China: new perspectives. Journal of Asian Earth Sciences 35, 334–353.
Song, S.G., Niu, Y.L., Su, L., Xia, X.H., 2012. Tectonics of the North Qilian orogen, NW China. Gondwana Research.
Spandler, C., Hermann, J., Arculus, R., Mavrogenes, J., 2003. Redistribution of trace elements during prograde metamorphism from lawsonite blueschist to eclogite facies; implications for deep subduction-zone processes. Contributions to Mineralogy and Petrology 146, 205–222.
Spandler, C., Hermann, J., Arculus, R., Mavrogenes, J., 2004. Geochemical heterogeneity and element mobility in deeply subducted oceanic crust; insights from high-pressure mafic rocks from New Caledonia. Chemical Geology 206, 21–42.
Staudigel, H., Davies, G.R., Hart, S.R., Marchant, K.M., Smith, B.M., 1995. Large scale isotopic Sr, Nd and O isotopic anatomy of altered oceanic crust: DSDP/ODP sites 417/418. Earth and Planetary Science Letters 130, 169–185.

Stolper, E., Newman, S., 1994. The role of water in the petrogenesis of Mariana Trough magmas. Earth and Planetary Science Letters 121, 293–325.
Sun, S.S., McDonough, W.F., 1989. Chemical and isotopic systematic in ocean basalt: implication for mantle composition and processes. Magmatism in the ocean Basins 313–345.
Tamura, Y., Tani, K., Chang, Q., Shukuno, H., Kawabata, H., Ishizuka, O., Fiske, R.S., 2007. Wet and dry basalt magma evolution at Torishima Volcano, Izu–Bonin Arc, Japan: the possible role of phengite in the downgoing slab. Journal of Petrology 48, 1999–2031.
Tatsumi, Y., 1986. Formation of the volcanic front in subduction zones. Geophysical Research Letters 13, 717–720.
Tatsumi, Y., Eggins, S., 1995. Subduction zone magmatism. Blackwell, Cambridge.
Tatsumi, Y., Kogiso, T., 1997. Trace element transport during dehydration processes in the subducted oceanic crust: 2. Origin of chemical and physical characteristics in arc magmatism. Earth and Planetary Science Letters 148, 207–221.
Tseng, C.Y., Yang, H.J., Yang, H.Y., Liu, D.Y., Tsai, C.L., Wu, H.Q., Zuo, G.C., 2007. The Dongcaohe ophiolite from the North Qilian Mountains: a fossil oceanic crust of the Paleo-Qilian ocean. Chinese Science Bulletin 52, 2390–2401.
van der Straaten, F., Schenk, V., John, T., Gao, J., 2008. Blueschist-facies rehydration of eclogites (Tian Shan, NW-China): implications for fluid–rock interaction in the subduction channel. Chemical Geology 255, 195–219.
Wang, C.Y., Zhang, Q., Qian, Q., Zhou, M.F., 2005. Geochemistry of the Early Paleozoic Baiyin volcanic rocks (NW China): implications for the tectonic evolution of the North Qilian Orogenic Belt. Journal of Geology 113, 83–94.
Whitney, D.L., Evans, B.W., 2010. Abbreviations for names of rock-forming minerals. American Mineralogist 95, 185–187.
Wu, H.Q., Feng, Y.M., Song, S.G., 1993. Metamorphism and deformation of blueschist belts and their tectonic implications, North Qilian Mountains, China. Jounal of Metamorphic Geologist 11, 523–536.
Xia, X.H., Song, S.G., 2010. Forming age and tectono-petrogenises of the Jiugequan ophiolite in the North Qilian Mountain, NW China. Chinese Science Bulletin 55, 1899–1907.
Xia, L.Q., Xia, Z.C., Xu, X.Y., 2003. Magmagenesis in the Ordovician backarc basins of the northern Qilian Mountains, China. Geological Society of Ameirca Bulletin 115, 1510–1522.
Xia, X.H., Song, S.G., Niu, Y.L., 2012. Tholeiite–Boninite terrane in the North Qilian suture zone: Implications for subduction initiation and back-arc basin development. Chemical Geology 328, 259–277.
Xiao, Y., Lavis, S., Niu, Y., Pearce, J.A., Li, H., Wang, H., Davidson, J., 2012. Trace element transport during subduction-zone ultrahigh pressure metamorphism: evidence from Western Tianshan, China. Geological Society of America Bulletin 124, 1113–1129.
Yang, J., Xu, Z., Zhang, J., Song, S., Wu, C., Shi, R., Li, H., Maurice, B., 2002. Early Palaeozoic North Qaidam UHP metamorphic belt on the north-eastern Tibetan plateau and a paired subduction model. Terra Nova 14, 397–404.
Zack, T., John, T., 2007. An evaluation of reactive fluid flow and trace element mobility in subducting slabs. Chemical Geology 239, 199–216.
Zhang, J.X., Meng, F.C., 2006. Lawsonite-bearing eclogites in the north Qilian and north Altyn Tagh: evidence for cold subduction of oceanic crust. Chinese Science Bulletin 51, 1238–1244.
Zhang, J.X., Xu, Z.Q., Chen, W., Xu, H.F., 1997. A tentative discussion on the ages of the subduction–accretionary complex/volcanic arcs in the middle sector of North Qilian Mountain. Acta Petrologica et Mineralogica 16, 112–119.
Zhang, J.X., Meng, F.C., Wan, Y.S., 2007. A cold Early Palaeozoic subduction zone in the North Qilian Mountains, NW China: petrological and U–Pb geochronological constraints. Journal of Metamorphic Geology 25, 285–304.
Zhang, L.F., Wang, Q., Song, S.G., 2009. Lawsonite blueschist in Northern Qilian, NW China: P–T pseudosections and petrologic implications. Journal of Asian Earth Science 35, 354–366.